Astrocyte Kir4.1 ion channel deficits contribute to neuronal dysfunction in Huntington's disease model mice

*[1]Xiaoping Tong, *[2]Yan Ao, [3]Guido C. Faas, [4]Sinifunanya E. Nwaobi, [1]Ji Xu, [1]Martin D. Haustein, [2]Mark A. Anderson, [1,3]Istvan Mody, [4]Michelle L. Olsen, [2]Michael V. Sofroniew[Ψ] & [1,2]Baljit S. Khakh[Ψ]

[1]Departments of Physiology, [2]Neurobiology and [3]Neurology, David Geffen School of Medicine, University of California Los Angeles, Los Angeles USA CA 90095-1751,
and
[4]Department of Cell, Developmental and Integrative Biology, University of Alabama at Birmingham, Birmingham, AL 35294

***authors with equal contributions to experiments (XT and YA)**

Supplementary information

15 figures

4 tables

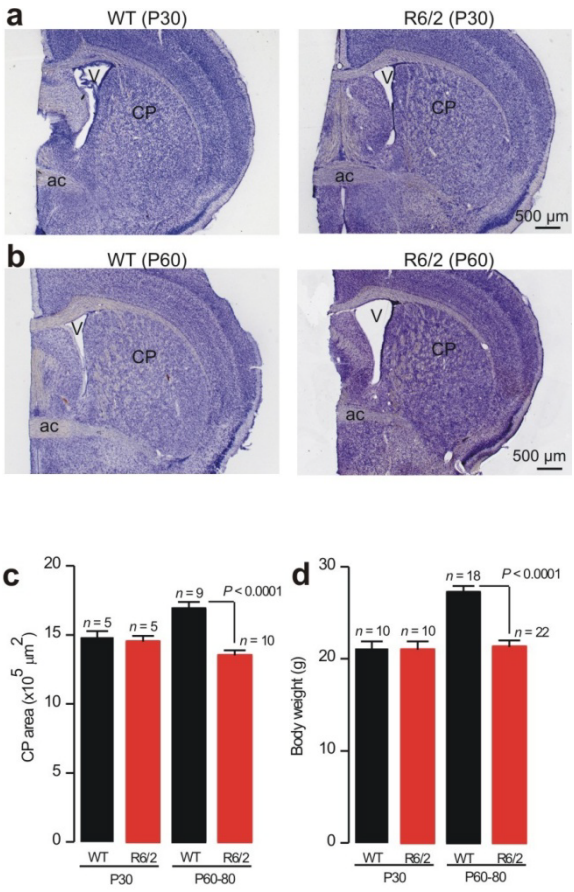

Supplemental Fig. 1: Basic characterization of R6/2 mice. a-b. Nissl (cresyl violet) stained brain sections from WT and R6/2 mice at P30 (**a**) and P60 (**b**). Note, at P60, when R6/2 mice display HD-like symptoms, the volume of the caudate putamen (CP) is reduced leading to enlarged ventricles (V). **c.** Quantification of the reduced CP area in R6/2 mice relative to WT and P60. **d.** R6/2 mice weighed less than their WT littermates at P60. Significance was assessed with an unpaired Student's *t* test; *P* values are shown.

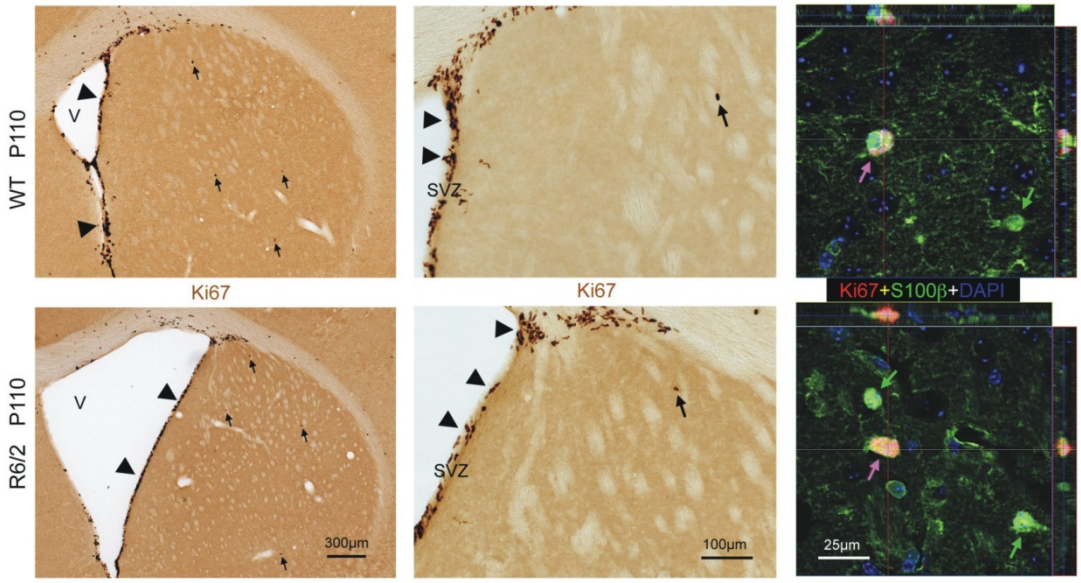

Supplemental Fig. 2: Ki67 IHC in WT and R6/2 mice.
Ki67 IHC in WT and R6/2 mice at P110 shows that many proliferating cells were seen in the subventricular zone (arrow heads), but few were seen in the striatum (arrows). In this regard, there were no differences between WT and R6/2 mice at P60-70 or P100. Some, but not all, Ki67 positive cells in the striatum colocalized with S100β, indicating that we were able to detect proliferating reactive astrocytes but that almost none were present.

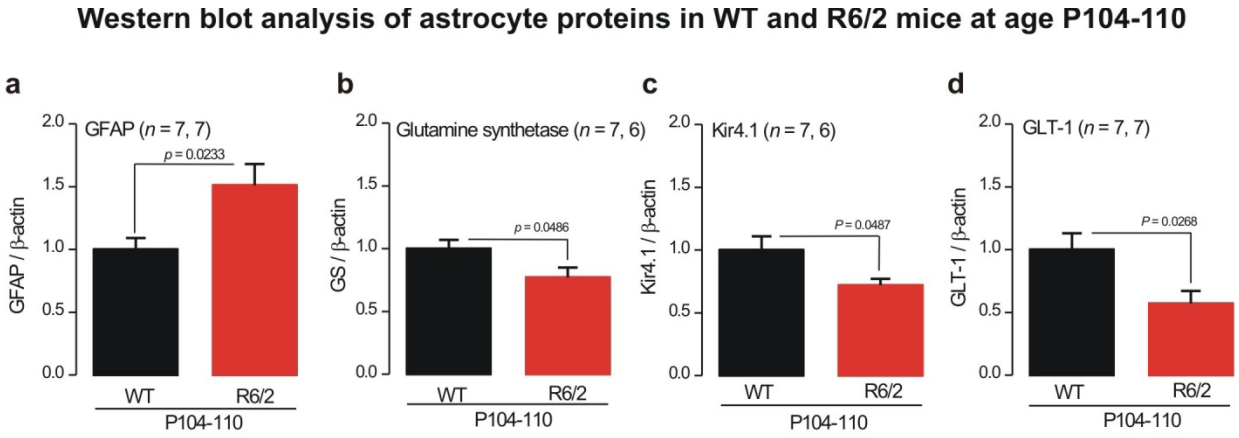

Supplemental Fig. 3: Western blot analysis of protein expression in striatal tissue at P104-110 for WT and R6/2 mice. Statistical significance was assessed with an unpaired Student's *t* test. n indicates the number of animals from each group. *P* values are shown.

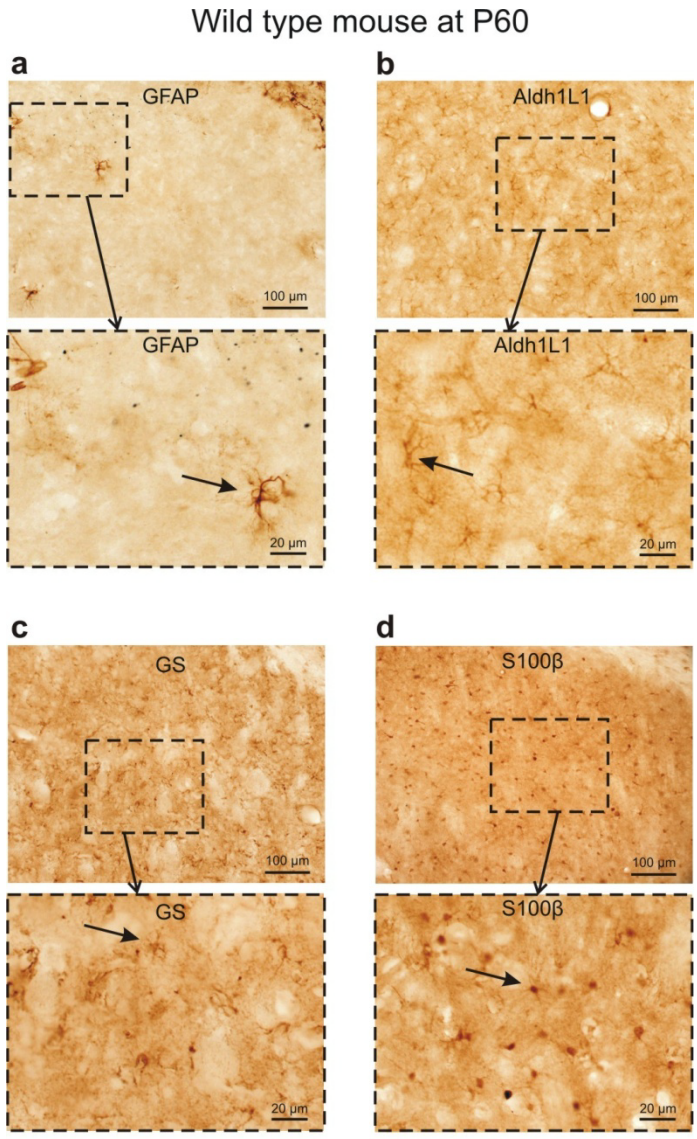

Supplemental Fig. 4: Labeling of striatal astrocytes with four commonly used astrocyte markers. GFAP (**a**), Aldh1L1(**b**), Glutamine synthetase (GS) (**c**) and S100β (**d**) in WT mouse at P60. As shown in **a**, only a few astrocytes were labeled with GFAP antibodies compared with the other three astrocyte markers. The images in the lower panels show higher magnification views from the boxes marked in the upper panels in each group.

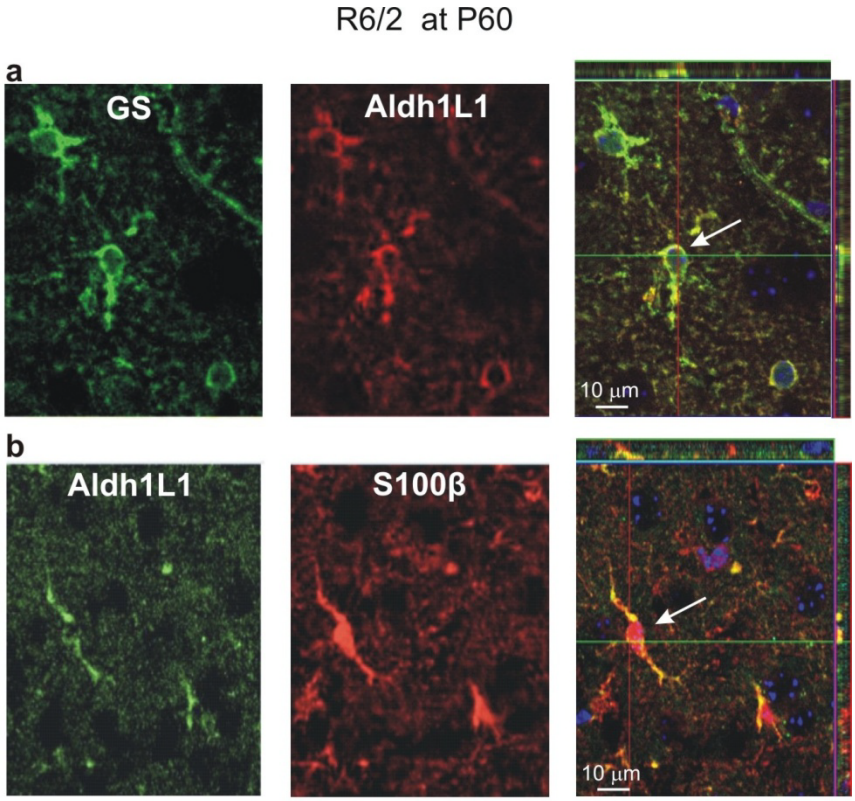

Supplemental Fig. 5: Colocalization of astrocyte markers in striatum of R6/2 mice at P60. (**a)** Shows glutamine synthetase (GS; green) colocalized with Aldh1 (red) in an astrocyte shown with an arrow. (**b**) As in (**a**), but for Aldh1L1 (green) colocalized with S100β (red).

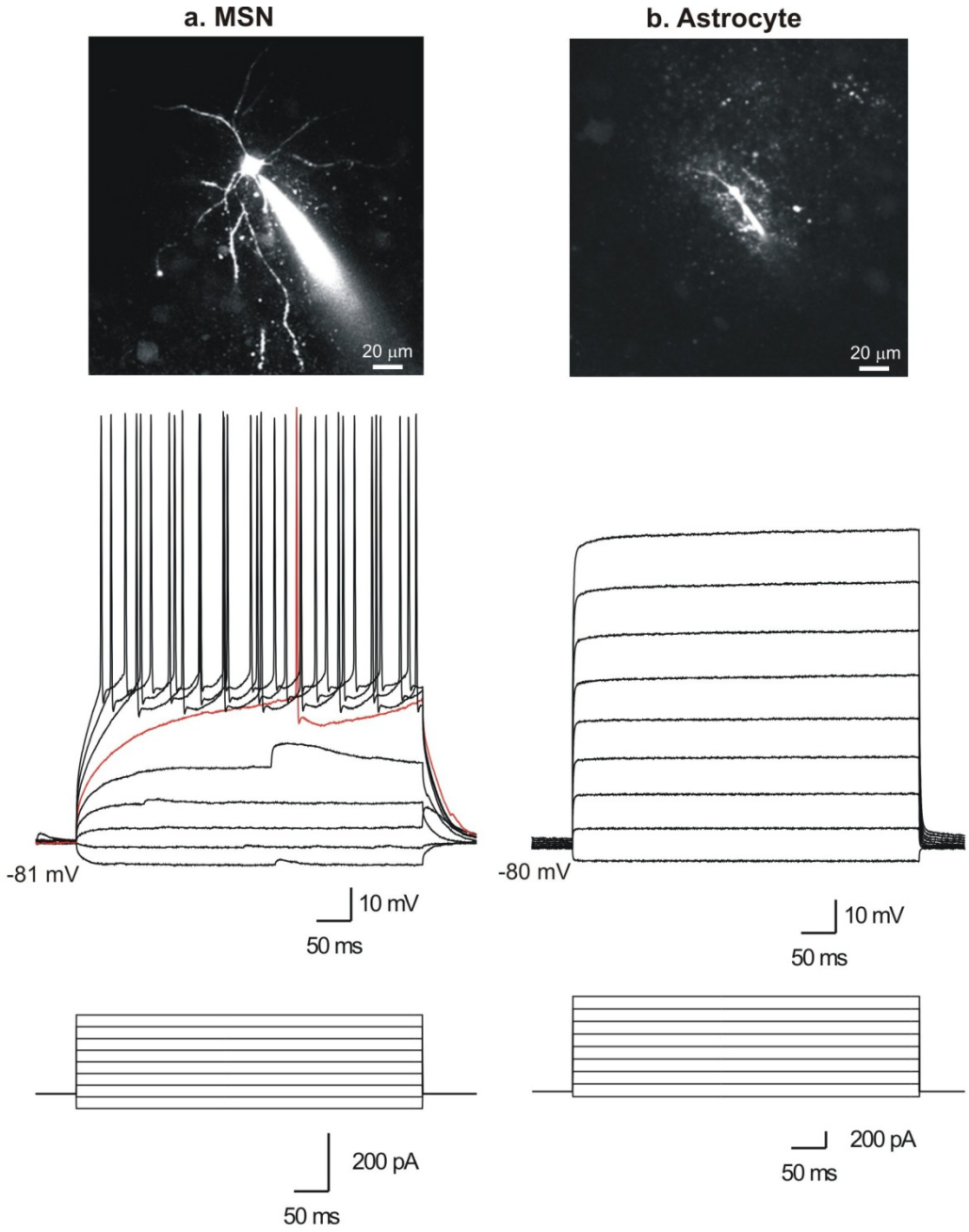

Supplemental Fig. 6: Basic properties of medium spiny neurons and astrocytes. Medium spiny neurons (MSN) and astrocytes in the striatum were easily distinguished during whole-cell recordings with Alexa 488 fluorescent dye in the pipette solution. (**a**) Shows a typical dendritic morphology of a MSN dialyzed with Alexa 488 (50 µM) for 30 min and the electrophysiological traces below show a negative resting membrane potential (-81 mV) and action potential firing during small depolarizing current injections. (**b**) Shows an astrocyte identically dialyzed with Alexa 488: a few short processes can be seen with a generally bushy appearance. The electrophysiological traces below show a negative resting membrane potential (-80 mV), but no action potential firing even for large depolarizing current injections.

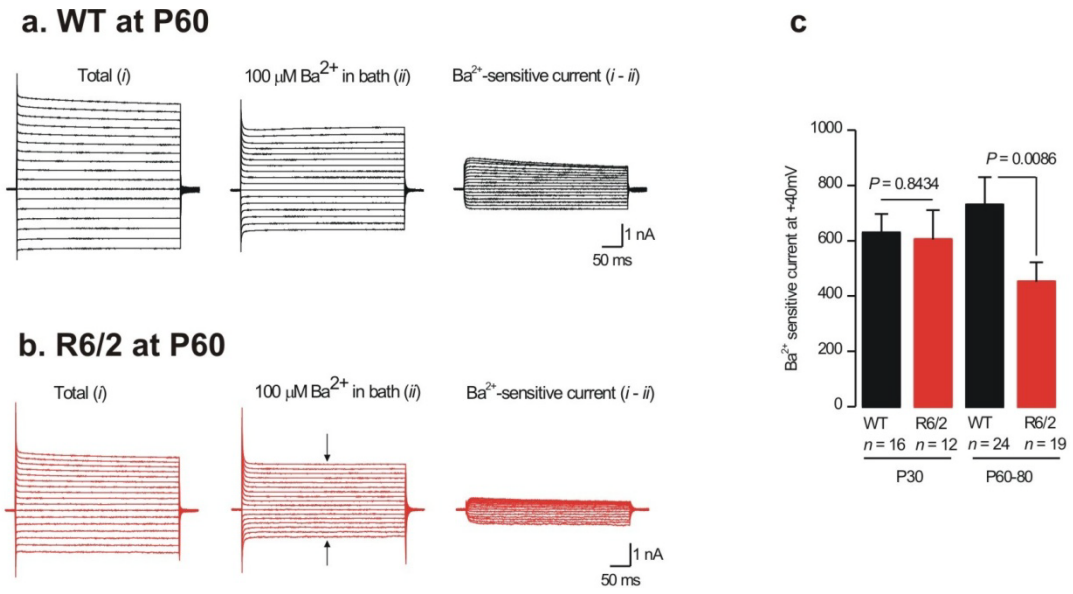

Supplemental Fig. 7: Barium sensitive currents. Representative traces showing total macroscopic currents (***i***), Ba^{2+}- insensitive currents (in 100 µM Ba^{2+} in the bath; ***ii***) and Ba^{2+}-sensitive currents (***i-ii***) recorded by whole-cell voltage clamp (from -120 mV to 40 mV) for striatal astrocytes from WT (**a**) and R6/2 mice (**b**) at P60. **c**. Note on average that the Ba^{2+}-sensitive current is smaller in R6/2 astrocytes than that in WT astrocytes at P60-80.

a. Kir4.1 levels relative to other mRNAs in WT and R6/2 mice at age P60-80

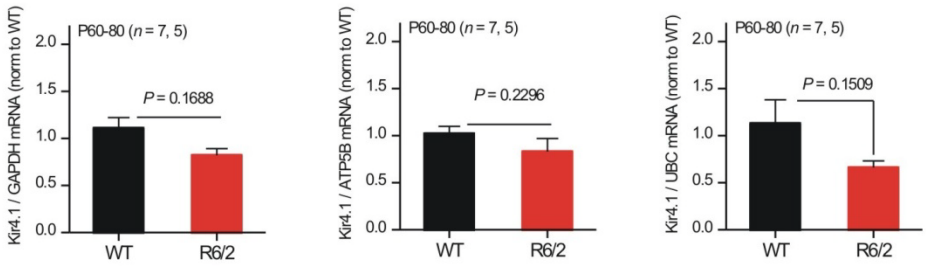

b. Kir4.1, GFAP and GLT-1 mRNA levels relative to GAPDH in Q175 mice

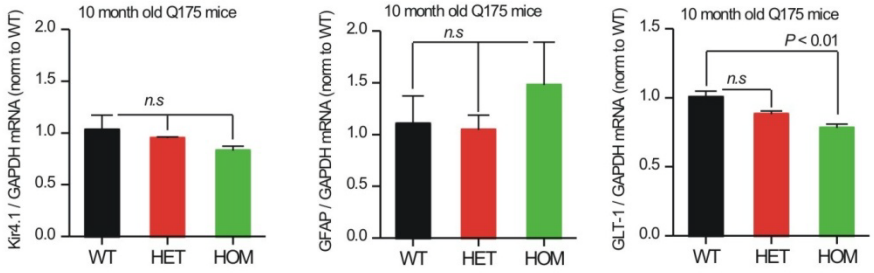

c. Kir4.1 mRNA levels relative to other mRNAs in Q175 mice

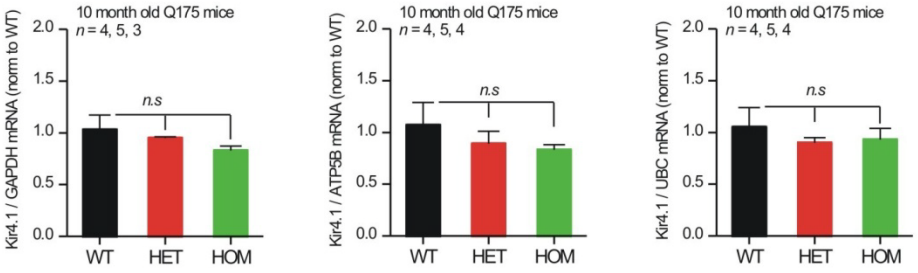

Supplemental Fig. 8: qPCR analyses.
a. Kir4.1 (*KCNJ10*) qPCR data for R6/2 and WT mice at P60-80 relative to three control mRNAs (GAPDH, ATP5B, and UBC). There were no significant differences when the data were assessed using un paired Student's *t* tests. *P* values are shown. **b.** qPCR data for Q175 mice aged 10 months for Kir4.1, GFAP and GLT-1. Only mRNA levels for GLT-1 were significantly different to WT controls. Statistical significance was assessed using an unpaired Student's *t* test; *P* values are shown. The experiments were done on 4-5 mice. **c.** Kir4.1 (*KCNJ10*) qPCR data for Q175 and WT mice at 10 months age relative to three control mRNAs (GAPDH, ATP5B, and UBC). There were no significant differences when the data were assessed using un paired Student's *t* tests. *P* values are shown.

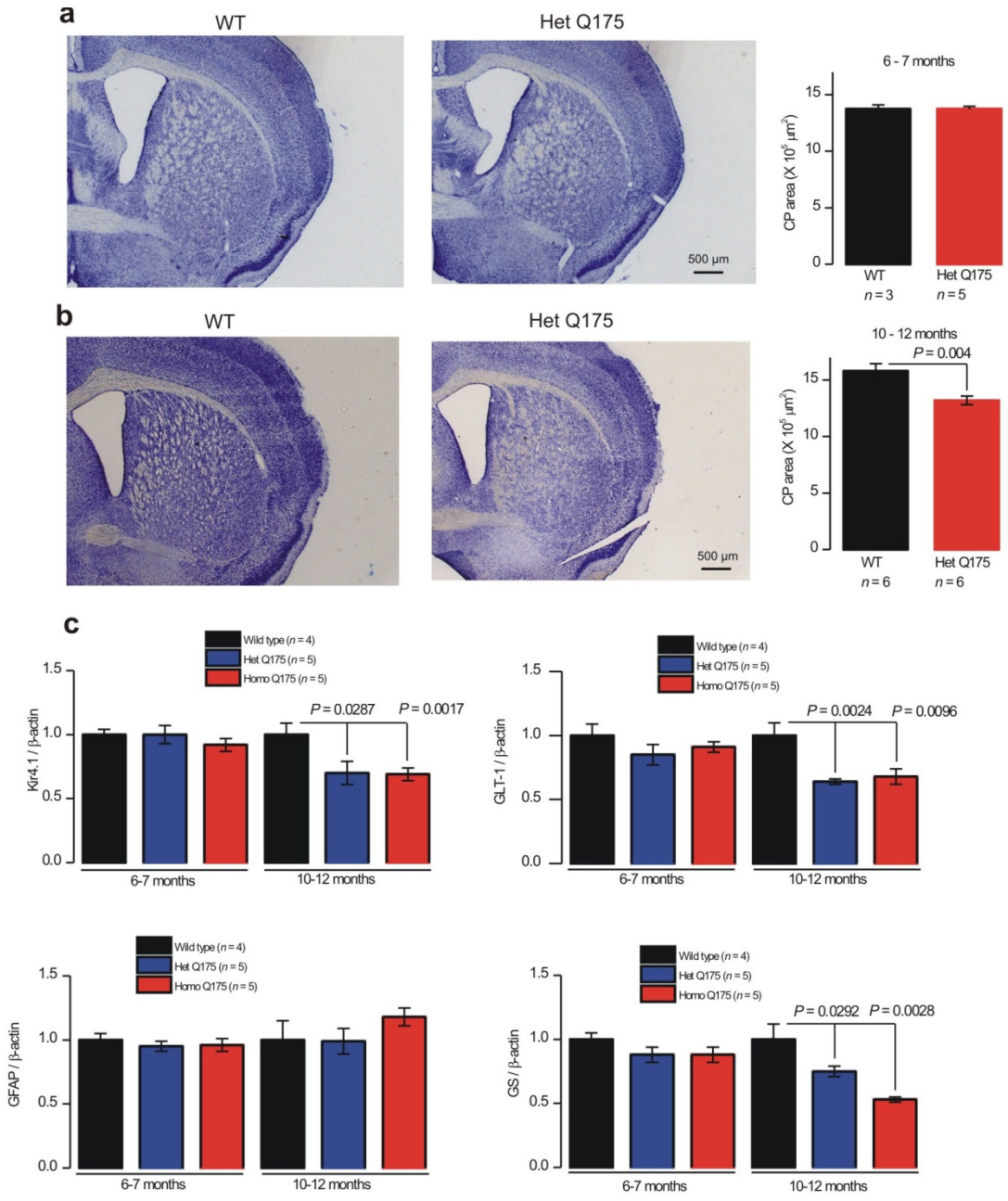

Supplemental Fig. 9: Characterization of Q175 mice. Representative images show there no CP volume change in wild type mice and heterozygous Q175 mice by Nissl staining at 6-7 months. Bar graph in right summaries the striatal area between two groups. (**B**) Representative images show decrease of the striatal volume in heterozygous Q175 mice at 12 months compared with comparative wild type mice. Bar graph in right shows the significant decrease of striatal areas in heterozygous Q175 mice. (**C**) Summary of western blots of Kir4.1, glutamine synthetase (GS), GLT-1 and GFAP protein expression levels in striatums of wild type, heterozygous and homozygous Q175 mice at 6-7 months and 9-12 months. Statistical tests were done using un paired Student's *t* tests; *p* values are shown. n indicates the number of animals in each group.

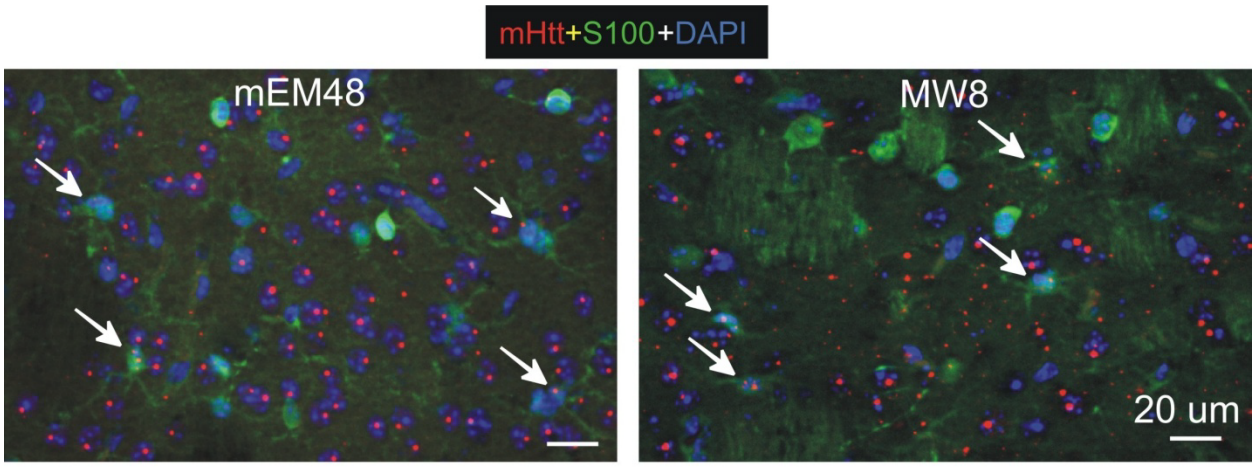

Supplemental Fig. 10: Representative images for IHC using two antibodies against mHTT (mEM48 and MW8). Both labeled nuclear inclusions in S100β labeled astrocytes to an equivalent degree. Neither is able to label cytoplasmic mHTT.

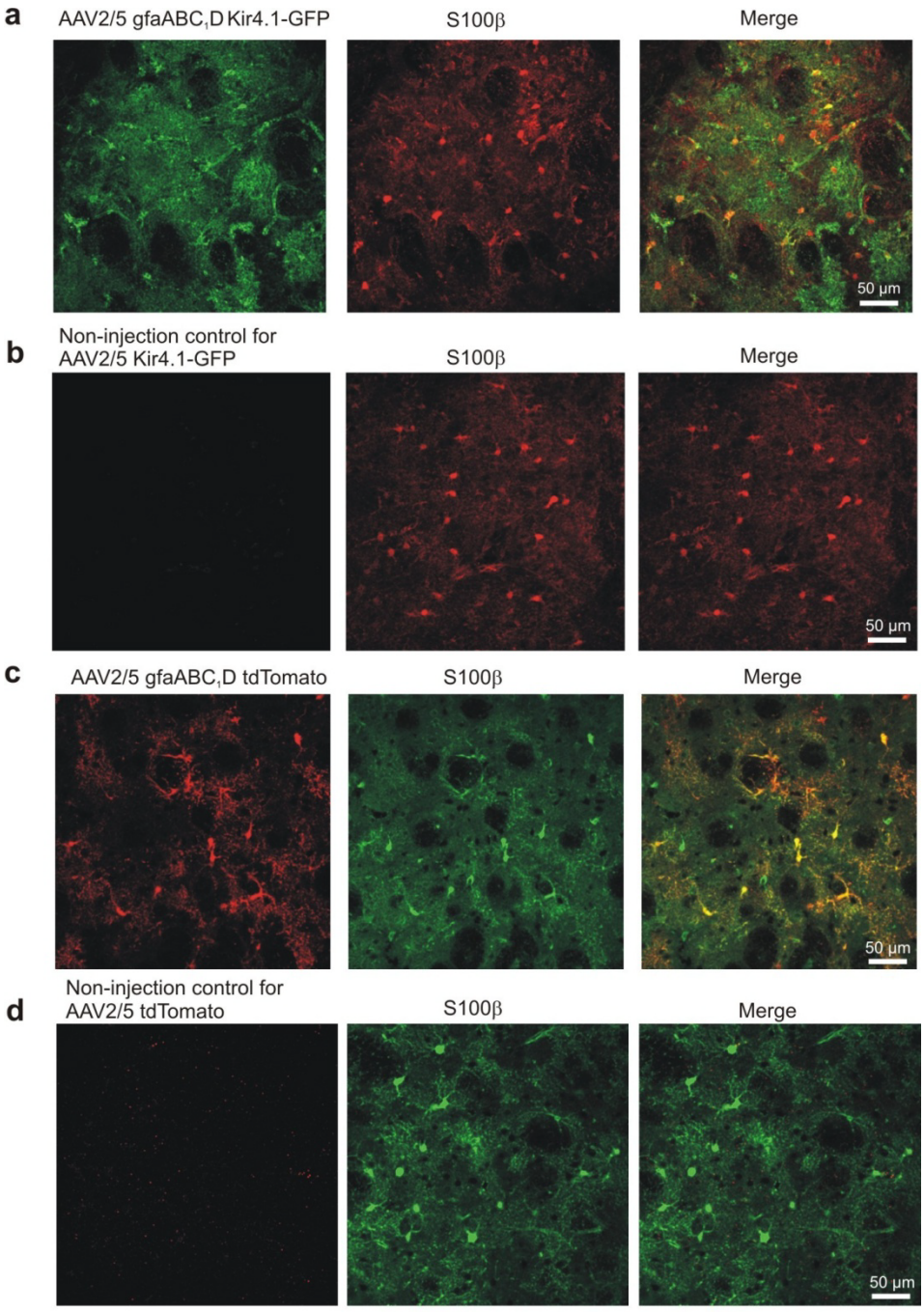

Supplemental Fig. 11: Representative images show S100β immunostaining in striatal tissue from R6/2 mice injected with AAV2/5 gfaABC$_1$D Kir4.1-GFP virus (a) or AAV2/5 gfaABC$_1$D tdTomato virus (c) at P56. Slice sections were collected for immunohistochemistry two weeks after viral injections at P56. Panels (**a)** and (**c)** show colocalization of S100β labeled astrocytes with Kir4.1-GFP and tdTomato positive cells, respectively. Controls from mice that received no virus injections (**b** and **d**) showed no colocalisation, but still showed S100β staining.

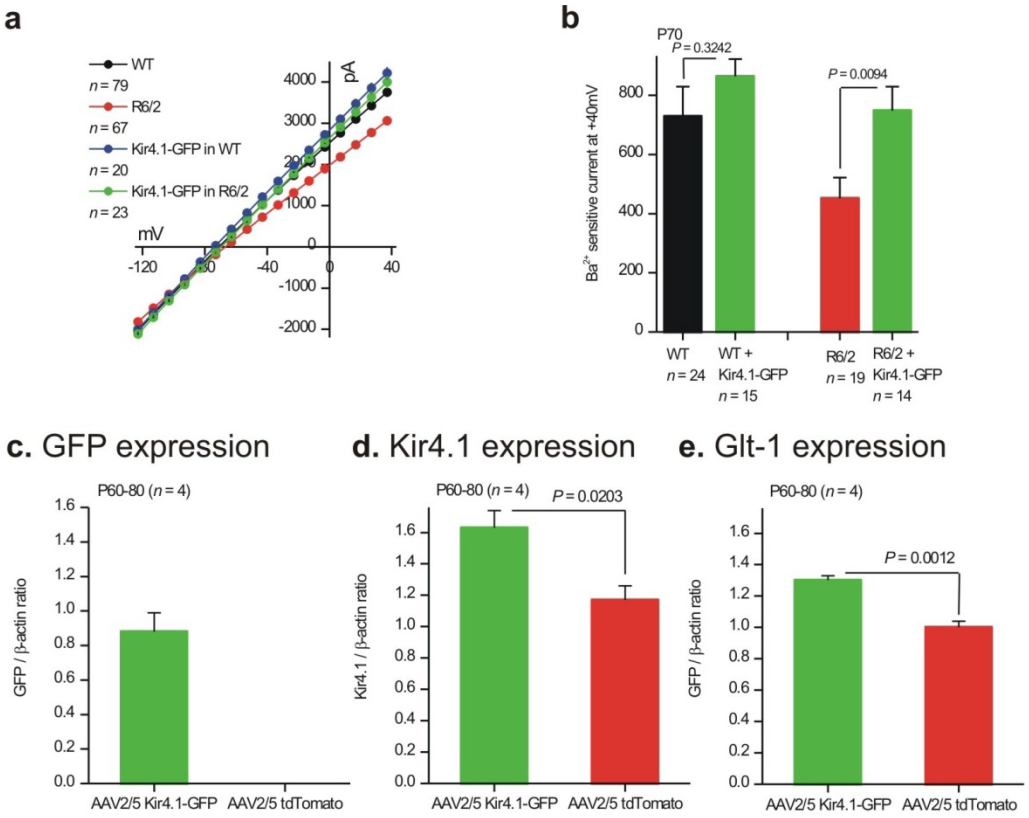

Supplemental Fig. 12: Controls for AAV2/5 Kir4.1-GFP. a. Astrocyte current-voltage (IV) relations. AAV2/5 Kir4.1-GFP expression in R6/2 mice increases the slope of the astrocyte IV relations and restores them to WT levels. However, Kir4.1-GFP expression in WT astrocytes did not boost the IV relations higher than WT levels. **b.** Ba^{2+} sensitive currents under the conditions shown. **c-e.** Western blot analysis from R6/2 mice injected with AAV2/5 for Kir4.1-GFP or AAV2/5 tdTomato. The Western blot data are for GFP (**c**) total Kir4.1 (**d**) and Glt-1 (**e**). Statistical differences were assessed using un paired Student's *t* tests. *P* values are shown.

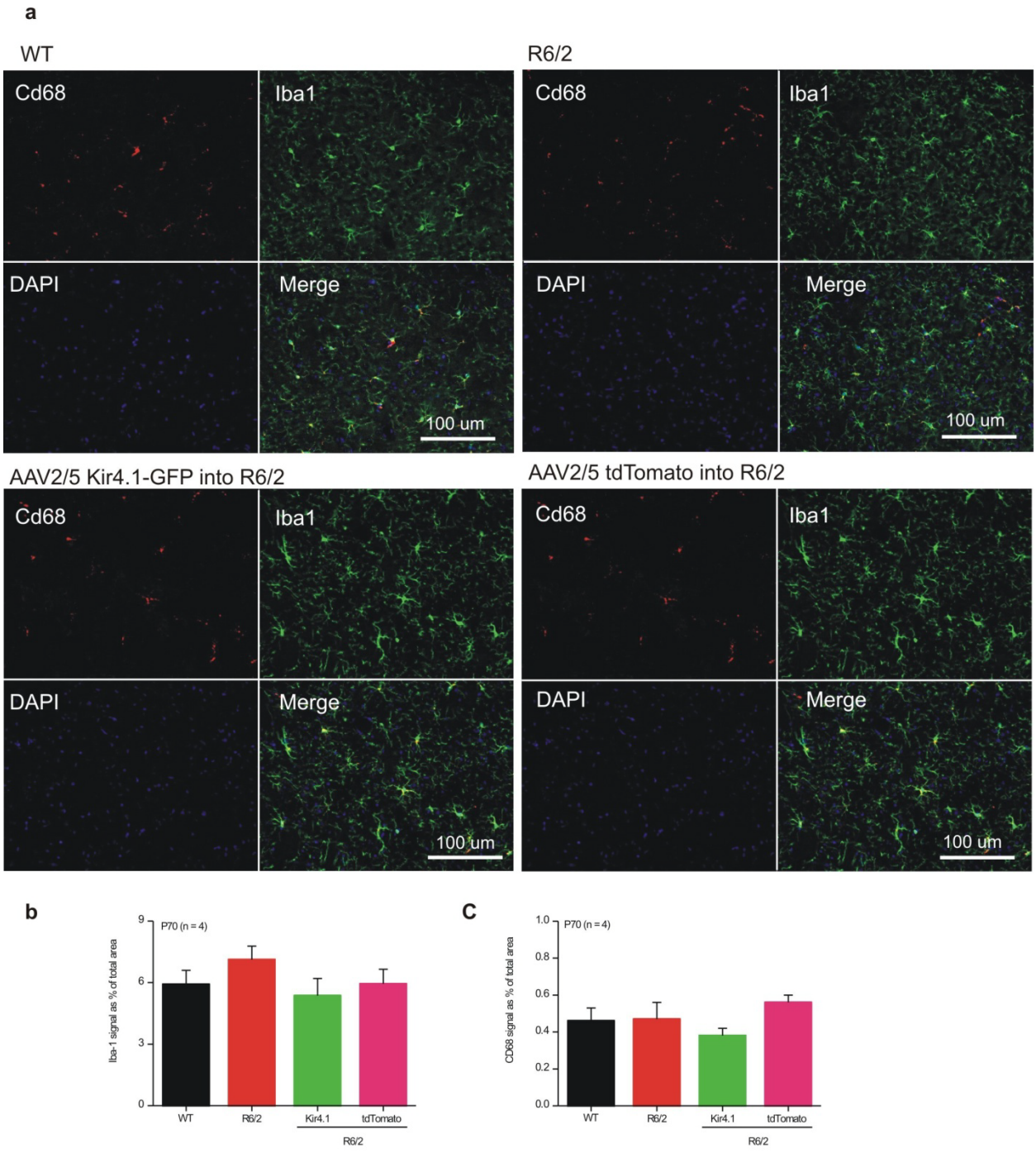

Supplemental Fig. 13: Assessment of inflammation. a. Representative images for Iba1 and CD68 IHC under the conditions shown. **b-c.** Summary data for Iba1 and CD68 IHC for experiments such as those shown in a. No qualitative or quantitative differences are detectable in staining intensity for inflammatory markers when comparing mice that received AAV2/5Kir4.1-GFP or AAV2/5-tdTomato.

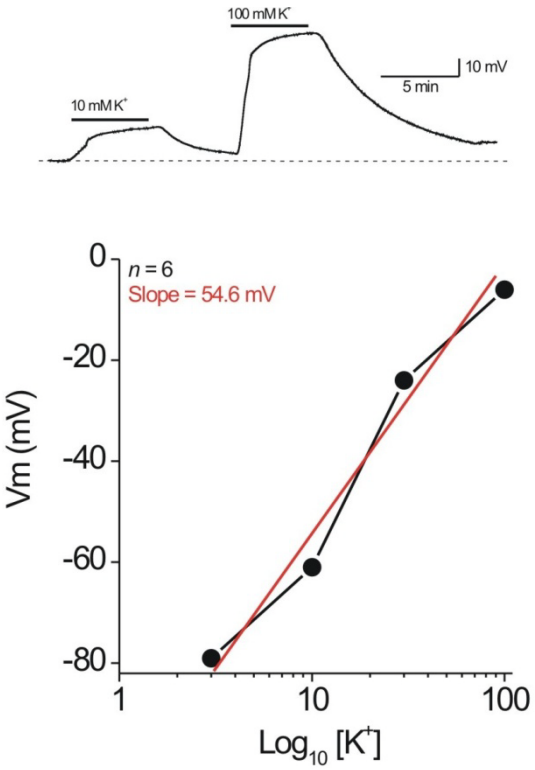

Supplemental Fig. 14: Representative trace and average data for the astrocyte membrane potential in different concentrations of bath K^+. The slope of the line shows a 55 mV depolarization for a 10-fold change in K^+ concentration. **Additional Note:** A salient feature across mouse models of HD is that MSNs display depolarized membrane potentials by as much as ~12 mV. A vaguely formulated idea suggests that reducing astrocyte Kir4.1 function with Ba^{2+} in WT slices may reveal secondary consequences for MSNs, i.e., this approach will elevate K^+ near neurons, depolarize MSNs and thus reveal astrocyte Kir4.1 contributions to altered MSN properties frequently observed in mouse models of HD. However, this view has problems. First, although Ba^{2+} is a useful tool to isolate astrocyte Kir4.1 currents, it also blocks MSN K^+ channels, meaning that it will be impossible to tell if any measured effects are due to Ba^{2+} actions on astrocytes or MSNs directly. Second, the suggested experiment can only work if brain slices can buffer K^+ locally, i.e. that local K^+ is not set by the bath K^+ concentration. We tested for this by measuring the astrocyte membrane potential in bath solutions of different K^+ concentration, exploiting the fact that astrocytes function as K^+ microelectrodes because of their high K^+ conductance. The Nernst equation predicts that the membrane potential of an astrocyte with a high K^+ conductance should change by ~56 mV for a ten-fold change in bath K^+ concentration. If brain slices can in fact buffer K^+ in the vicinity of a cell, then we would predict a deviation from this, because the local K^+ concentration would be set by buffering and not by the bath K^+ concentration. We found that striatal astrocytes showed a near perfect Nernst-like ~55 mV depolarization for a 10-fold change in bath K^+ concentration. These data show that isolated preparations such as brain slices cannot buffer K^+. Thus, the idea of blocking astrocyte Kir4.1 channels with Ba^{2+} and looking for downstream effects on MSNs because of disrupted local K^+ buffering is flawed.

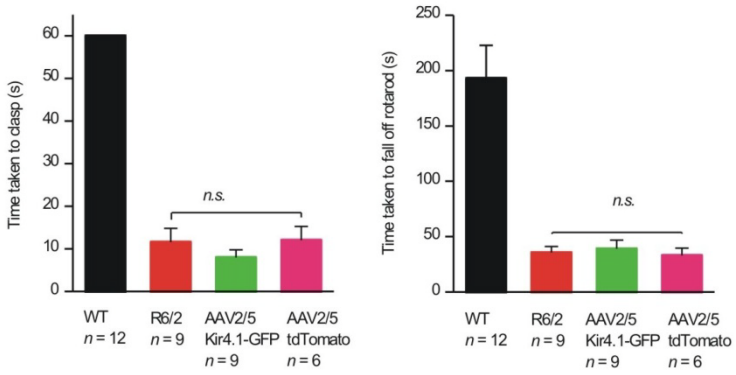

Supplemental Fig 15: Average data for behavioral analysis. R6/2 mice injected with AAV2/5 for Kir4.1-GFP were not different to R6/2 mice or to R6/2 mice injected with AAV2/5 for tdTomato in assays that measured motor function (forelimb clasp time and the time to fall off a rotarod). The clasp time experiments were conducted over 1 min. Since the WT mice did not clasp in this time period, their data values are all at 60 s.

Supplementary Table 1: Electrophysiological properties of striatal and hippocampal astrocytes from WT and R6/2 mice at P30 and P60-80

	P30 striatal astrocytes		P60-80 striatal astrocytes	
	Wild type	**R6/2**	**Wild type**	**R6/2**
Control conditions				
Resting membrane potential (mV)	-76 ± 1	-76 ± 1	-76 ± 1	-71 ± 1** ($P < 0.0001$)
Membrane resistance (MΩ)	26 ± 1	27 ± 1	29 ± 1	35 ± 2** ($P < 0.0001$)
Membrane conductance (nS)	40 ± 1	39 ± 1	37 ± 1	31 ± 1** ($P < 0.0001$)
Membrane access resistance (MΩ)	21 ± 0.5	22 ± 0.5	22 ± 0.5	23 ± 1
Body weight of mouse (g)	18 ± 1	19 ± 1	27 ± 0.5	22 ± 1** ($P < 0.0001$)
Number of cells recorded (number of mice)	53 (15)	55 (16)	79 (27)	67 (23)
Ba^{2+}-sensitive responses				
Peak Ba^{2+}-sensitive currents at +40 mV (pA)	629 ± 69	605 ± 106	730 ± 100	452 ± 71** ($P = 0.0086$)
Number of cells recorded (number of mice)	16 (5)	12 (6)	24 (15)	19 (12)
	P30 hippocampal astrocytes		**P60-80 hippocampal astrocytes**	
	Wild type	**R6/2**	**Wild type**	**R6/2**
Control conditions				
Resting membrane potential (mV)	-76 ± 1	-74 ± 1	-76 ± 1	-76 ± 1
Membrane resistance (MΩ)	25 ± 1	25 ± 2	28 ± 2	28 ± 1
Membrane conductance (nS)	42 ± 3	43 ± 4	37 ± 2	37 ± 2
Membrane access resistance (MΩ)	21 ± 1	21 ± 2	23 ± 1	22 ± 1
Body weight of mouse (g)	18 ± 1	21 ± 2	27 ± 3	22 ± 1
Number of cells recorded (number of mice)	19 (9)	10 (5)	10 (3)	11 (4)
Ba^{2+}-sensitive responses				
Peak Ba^{2+}-sensitive currents at +40 mV (pA)	502 ± 77	537 ± 55	448 ± 107	469 ± 106
Number of cells recorded (number of mice)	11 (7)	7 (5)	10 (4)	9 (4)

Note for table: Here, * indicates $P < 0.05$ and ** indicates $P < 0.01$ with two tailed Mann-Whitney tests relative to WT. P values are indicated.

Supplementary Table 2: Electrophysiological properties of striatal astrocytes from WT and Q175 mice at 2-3 and 6-7 months of age.

	Mice aged 2-3 months		
	WT	Heterozygous Q175	Homozygous Q175
Control conditions			
Resting membrane potential (mV)	-76 ± 1	-78 ± 1	-74 ± 2
Membrane resistance (MΩ)	25 ± 1	25 ± 1	25 ± 1
Membrane conductance (nS)	42 ± 2	40 ± 2	41 ± 2
Access resistance (MΩ)	20 ± 1	19 ± 1	20 ± 1
Body weight of mouse (g)	22 ± 1	20 ± 1	18 ± 2
Number of cells recorded (number of mice)	18 (8)	12 (5)	20 (7)
Ba^{2+}-sensitive responses			
Peak Ba^{2+}-sensitive currents at +40 mV (pA)	568 ± 92	794 ± 87	465 ± 46
Number of cells recorded (number of mice)	11 (7)	12 (5)	16 (7)
	Mice aged 6-7 months		
	WT	Heterozygous Q175	Homozygous Q175
Control conditions			
Resting membrane potential (mV)	-76 ± 1	-74 ± 1	-71 ± 1** ($P < 0.0001$)
Membrane resistance (MΩ)	23 ± 1	24 ± 1	26 ± 1
Membrane conductance (nS)	47 ± 2	44 ± 2	41 ± 2* ($P = 0.0293$)
Access resistance (MΩ)	18 ± 1	20 ± 1	21 ± 1
Body weight of mouse (g)	29 ± 2	25 ± 2	22 ± 2** ($P = 0.0048$)
Number of cells recorded (number of mice)	45 (12)	33 (10)	26 (9)
Ba^{2+}-sensitive responses			
Peak Ba^{2+}-sensitive currents at +40 mV (pA)	664 ± 52	644 ± 83	446 ± 69* ($P = 0.0179$)
Number of cells recorded (number of mice)	34 (12)	26 (10)	17 (9)

Note for table: at 2-months for Q175 mice, there were no significant differences between WT, heterozygous and homozygous mice for the variables listed. At 6-7 months for Q175 mice, there were some significant differences between WT, heterozygous and homozygous mice for the variables listed. These differences were most notable for the homozygous mice. Here, * indicates $P < 0.05$ and ** indicates $P < 0.01$ with an unpaired Student's *t* test relative to WT. *P* values are stated.

Supplementary Table 3: Electrophysiological properties of striatal astrocytes from WT and Q175 mice at 9-12 months of age.

	Mice aged 9-12 months		
	WT	Heterozygous Q175	Homozygous Q175
Control conditions			
Resting membrane potential (mV)	-74 ± 0.5	-71 ± 1** (P = 0.0042)	-70 ± 1** (P = 0.0003)
Membrane resistance (MΩ)	22 ± 1	26 ± 1** (P < 0.0001)	29 ± 2** (P < 0.0001)
Membrane conductance (nS)	46 ± 2	40 ± 2** (P = 0.008)	35 ± 2** (P < 0.0001)
Access resistance (MΩ)	20 ± 0.5	22 ± 1	25 ± 1
Body weight of mouse (g)	30 ± 2	27 ± 3	23 ± 2* (P = 0.0274)
Number of cells recorded (number of mice)	25 (8)	23 (6)	18 (5)
Ba^{2+}-sensitive responses			
Peak Ba^{2+}-sensitive currents at +40 mV (pA)	751 ± 95	453 ± 52* (P = 0.0108)	366 ± 56** (P = 0.0028)
Number of cells recorded (number of mice)	14 (7)	14 (6)	12 (5)

Note for table: at this age of Q175 mice, there were several significant differences between WT, heterozygous and homozygous mice for the variables listed. These differences were notable for the heterozygous and homozygous mice. Here, * indicates $P < 0.05$ and ** indicates $P < 0.01$ with an unpaired Student's t test relative to WT. P values are listed

Supplementary Table 4: Nortriptyline-sensitive currents in WT and R6/2 striatal astrocytes at P60-80.

	WT	R6/2
Control conditions		
Resting membrane potential (mV)	-75 ± 1	-71 ± 2** (P = 0.00477)
Membrane resistance (MΩ)	25 ± 1	28 ± 2
Membrane conductance (nS)	40 ± 2	37 ± 2
Membrane access resistance (MΩ)	21 ± 1	23 ± 1
Body weight of mouse (g)	29 ± 1.0	27 ± 0.3* (P = 0.0346)
Number of cells recorded (number of mice)	14 (5)	13 (5)
Nortriptyline-sensitive responses		
Peak currents at holding voltage of +40 mV (pA)	1089 ± 179	610 ± 62* (P = 0.0219)
Number of cells recorded (number of mice)	14 (5)	13 (5)

Note for table: Here, * indicates $P < 0.05$ with an unpaired Student's t test relative to WT.